Peridynamic modeling of rail squats

Freimanis, Andris; Kaewunruen, Sakdirat; Ishida, Makoto

DOI:
10.1007/978-3-030-01911-2_10

License:
Other (please specify with Rights Statement)

Document Version
Peer reviewed version

Citation for published version (Harvard):
Freimanis, A, Kaewunruen, S & Ishida, M 2018, Peridynamic modeling of rail squats. in S El-Badawy & J Valentin (eds), *Sustainable Solutions for Railways and Transportation Engineering.* Sustainable Civil Infrastructure, Springer, pp. 108-118, 2nd GeoMEast International Congress and Exhibition on Sustainable Civil Infrastructures, Egypt 2018, Cairo, Egypt, 24/11/18. https://doi.org/10.1007/978-3-030-01911-2_10

Peridynamic modeling of rail squats

Andris Freimanis[2], PhD; Sakdirat Kaewunruen[1], PhD and
Makoto Ishida[3], PhD

[1]PhD Candidate, Riga Technical University, Riga, Latvia. andris.freimanis_1@rtu.lv
[1]Senior Lecturer in Railway and Civil Engineering, School of Engineering, the University of Birmingham, Birmingham, United Kingdom, s.kaewunruen@bham.ac.uk
[3]Chief Track Engineer, Railway Engineering Department, Nippon Koei Ltd., Tokyo, Japan. ishida-mk@n-koei.jp

ABSTRACT: Rail squats and studs are typically classified as the propagation of any cracks that have grown longitudinally through the subsurface. Some of the cracks could propagate to the bottom of rails transversely, which have branched from the initial longitudinal cracks with a depression of rail surface. The rail defects are commonly referred to as 'squats' when they were initiated from damage layer caused by rolling contact fatigue, and as 'studs' when they were associated with white etching layer caused by the transform from pearlitic steel due to friction heat generated by wheel sliding or excessive traction. Such above-mentioned rail defects have been often observed in railway tracks catered for either light passenger or heavy freight traffics and for low, medium or high speed trains all over the world for over 60 years except some places such as sharp curves where large wear takes place under severe friction between wheel flange and rail gauge face. It becomes a much-more significant issue when the crack grows and sometimes flakes off the rail (by itself or by insufficient rail grinding), resulting in a rail surface irregularity. Such rail surface defect induces wheel/rail impact and large amplitude vibration of track structure and poor ride quality. In Australia, Europe and Japan, rail squats/studs have occasionally turned into broken rails. The root cause and preventive solution to this defect are still under investigation from the fracture mechanics and material sciences point of view. Some patterns of squat/stud development related to both of curve and tangent track geometries have been observed, and squat growth has also been monitored for individual squats using ultrasonic mapping techniques. This paper highlights peridynamic modeling of squat/stud distribution and its growth. Squat/stud growth has been measured in the field using the ultrasonic measurement device on a grid applied to the rail surface. The depths of crack paths at each grid node form a three dimensional contour of rail squat crack. The crack propagation of squats/studs is modelled using peridynamics. The modeling and field data is compared to evaluate the effectiveness of peridynamics in modelling rail squats.

INTRODUCTION

Rail squats, defined as cracks initiated from rolling contact fatigue (RCT) and from white etching layer (WEL); and growing longitudinally under the rail surface (in the direction to train), are a main problem for rail operators all around the globe. They are noticed by passengers when they create excess noise and vibration leading to uncomfortable rides (Remennikov and Kaewunruen 2008), but more importantly they can result in broken rail from the impact forces from wheel-rail interaction (Kaewunruen and Remennikov 2010, 2009). Additionally, squats have grown and

turned into broken rails, which could result in a catastrophe (Ishida 2013). In practice, the rail surface defects have been a critical safety concern and key maintenance priority of railway infrastructure owners and managers who operate either low, moderate or high speed trains including passenger suburban, metro, urban, mixed-traffic and freight rail systems. The rail surface defects can cause high risks and significant consequences such as train derailments from rail breaks, component failures, and so on. It has been estimated that the cost of rail renewal program (rail replacement) due to rail squats and studs has become a significant portion of the whole track maintenance cost, reportedly in Australia, Asia, and European countries e.g. Austria, Japan, Germany and France (Kaewunruen et al., 2015; Kaewunruen and Ishida, 2014; 2015; 2016). The rail squat/stud problem has largely been noticed when the ride quality of the passenger trains exceeds acceptable limits (Kaewunruen and Remennikov, 2016). Excessive noise and vibration have later increased complaints against rail operators. Most importantly, the impact forces due to the wheel/rail interaction have undermined the structural integrity and stability of track components (Remennikov and Kaewunruen, 2008). The study into innovative solutions for this problem is timely and significant. This paper is the world first to adopt peridynamic theory to predict dynamic crack growth from RCT, and to the best of authors' knowledge no other such work exists currently (Kaewunruen, 2015; 2018).

Classical mechanics theory uses spatial derivatives that do not exist in when the displacement field is discontinuous, so the techniques of fracture mechanics are used to study cracking phenomena. However, a major drawback is that crack path must be known *a priori*. Therefore, peridynamics (PD) (Silling 2000; Silling et al. 2007) was created to simulate objects with discontinuities. It uses integral not partial-differential equations, and deformation instead of strain to compute the internal forces. Since both are defined in the presence of cracks, PD are well suited for such analyses. Moreover, in PD crack path doesn't have to be known –cracks initiate automatically according to a prescribed damage law. These reasons make PD an excellent tool for studying different kinds of fracture and have been used to study damage in fiber-reinforced laminated composites (Colavito 2013; Hu, De Carvalho, and Madenci 2015; Hu, Madenci, and Phan 2017; Kilic, Agwai, and Madenci 2009), glass (Bobaru, Ha, and Hu 2012; Bobaru and Zhang 2016), wood (Perré et al. 2015), concrete (Gerstle, Sau, and Sakhavand 2009; Shen, Zhang, and Huang 2013; Yaghoobi and Chorzepa 2015) and steel (De Meo et al. 2016).

STATE-BASED PERIDYNAMICS

This section presents a brief overview of the state-based peridynamics theory, for an extended overview authors recommend (Bobaru et al. 2016; Madenci and Oterkus 2014; Silling and Lehoucq 2010). A peridynamic body consists of a number of nodes in the reference position $\boldsymbol{x_i}$ each describing some volume V_{x_i}. A node $\boldsymbol{x_i}$ interacts with other nodes $\boldsymbol{x_j}$ within a range called the horizon δ through bonds. Nodes within this range is called the family of $\boldsymbol{x_i}$, H_{x_i}, When a body undergoes some deformation, node $\boldsymbol{x_i}$ experiences displacement $\boldsymbol{u_i}$ and moves to a deformed position $\boldsymbol{y_i}$. This deformation creates a force density vector $\boldsymbol{t_{ij}}$ that depends on the collective deformation of H_{x_i} and $\boldsymbol{t_{ji}}$ that depends on the collective deformation of H_{x_j}. The bond deformation vectors

and the force density vectors are stored in arrays called the deformation states, $\mathbf{Y}_{x_i}$ and the force states $\mathbf{T}_{x_i}$:

$$\mathbf{Y}_{x_i} = \begin{Bmatrix} y_1 - y_i \\ \vdots \\ y_n - y_i \end{Bmatrix}, \mathbf{T}_{x_i} = \begin{Bmatrix} t_{i1} \\ \vdots \\ t_{in} \end{Bmatrix}. \tag{1}$$

It is common to write $\mathbf{T}(x_i)\langle x_j - x_i \rangle$ when referring to a force density vector t_{ij} in a specific bond $\xi_{ij} = x_j - x_i$. The force density vectors depend on the deformation, so we can write:

$$\mathbf{T}(x_i) = \mathbf{T}\big(\mathbf{Y}(x_i)\big) \tag{2}$$

where the function $\mathbf{T}(x_i)$ is the material model. Then the peridynamic equation of motion in the integral form is

$$\rho(x_i)\ddot{u}(x_i, t) = \int_{H_{x_i}} \big(\mathbf{T}(x_i)\langle x_j - x_i \rangle - \mathbf{T}(x_j)\langle x_i - x_j \rangle\big) dV_{x_j} + b(x_i) \tag{3}$$

where $\rho(x_i)$ – density, $\ddot{u}(x_i)$ – acceleration and $b(x_i)$ – external force density.

Boundary conditions are not required in PD solution, because the PD equation of motion does not contain any spatial derivatives, however, they are necessary to solve many real-life problems. Since nodes describe some volume, boundary conditions must also be applied to some volume.

Damage is introduced by breaking a bond. The simplest damage criterion could be the critical stretch, in which a bond breaks when it's stretched past some critical value s_c:

$$\omega(x_i) = \begin{cases} 1 & , \quad if\ s_{ij} < s_c \\ 0 & , \quad if\ s_{ij} \geq s_c \end{cases}, \quad s_{ij} = \frac{|y_j - y_i| - |x_j - x_i|}{|x_j - x_i|} = \frac{|\mathbf{Y}\langle \xi_{ij} \rangle| - |\xi_{ij}|}{|\xi_{ij}|}. \tag{4}$$

The damage at a node is defined in (Silling and Askari 2005) as a ratio between the broken and the initial number of bonds:

$$\phi(x_i) = 1 - \frac{\int_{H_{x_i}} \omega(x_i)\, dV_{\xi_{ij}}}{\int_{H_{x_i}} dV_{\xi_{ij}}}. \tag{5}$$

The PD fatigue damage model used in this study was introduced in (Silling and Askari 2014) and used in (Jung and Seok 2017, 2016; Zhang et al. 2016). Other researchers have also developed fatigue damage models (Baber and Guven 2017; Oterkus, Guven, and Madenci 2010), however, these models use bond-based PD and simulate only the crack growth phase. The overview of the model is given in (Silling and Askari 2014), but it's repeated here for completeness.

A body undergoes some cyclic deformation between two extremes + and -, bond strains at each extreme and the cyclic bond strain is:

$$s_{ij}^{+} = \frac{|\mathbf{Y}^{+}\langle \xi_{ij} \rangle| - |\xi_{ij}|}{|\xi_{ij}|}, \qquad s_{ij}^{-} = \frac{|\mathbf{Y}^{-}\langle \xi_{ij} \rangle| - |\xi_{ij}|}{|\xi_{ij}|}, \qquad \varepsilon_{ij} = |s_{ij}^{+} - s_{ij}^{-}|. \tag{6}$$

For each bond a variable called the "remaining life" $\lambda_{ij}(x_i, \xi_{ij}, N)$ is defined. It degrades at each loading cycle N, and a bond breaks when the remaining life is reduced to zero:

$$\lambda_{ij}(N) \leq 0. \tag{7}$$

At the beginning when $N = 0$:

$$\lambda_{ij}(0) = 1, \tag{8}$$

then at each cycle in crack nucleation phase (phase I) the change of λ is given by

$$\frac{d\lambda_{ij}}{dN}(N) = \begin{cases} -A_I\left(\varepsilon_{ij} - \varepsilon_\infty\right)^{m_I} & ,if\ \varepsilon_{ij} > \varepsilon_\infty \\ 0 & ,if\ \varepsilon_{ij} \le \varepsilon_\infty, \end{cases} \tag{9}$$

where ε_∞ - fatigue limit under which no fatigue damage occurs, A_I, m_I – parameters for phase I. In the phase II the remaining life changes according to:

$$\frac{d\lambda_{ij}}{dN}(N) = -A_{II}\varepsilon_{ij}^{m_{II}}. \tag{10}$$

The transition from phase I to phase II is handled by applying the phase I model with parameters A_I, m_I to a node $\boldsymbol{x_i}$ till there is a node $\boldsymbol{x_j}$ in H_{x_i} with damage

$$\phi(\boldsymbol{x_j}) \ge 0.5, \tag{11}$$

then reset the remaining life of the bonds connected to $\boldsymbol{x_i}$ to 1 and switch to phase II model.

COMPUTATIONAL MODEL

The fatigue damage model was implemented in the open-source Peridynamics program Peridigm (Lihlewood et al. 2013; Parks et al. 2012). For quasi-static analysis the acceleration is zero, so peridynamic equation of motion is approximated as:

$$\sum_{H_{x_i}} \left(T[x_i,t]\langle x_j - x_i\rangle - T\left[x_j,t\right]\langle x_i - x_j\rangle\right)\Delta V_{x_j} + b(x_i,t) = 0. \tag{12}$$

and then solved using Newton's method. The remaining life of each bond is computed after each simulation step, by:

$$\lambda_{i,j}^0 = 1,\ \ \lambda_{i,j}^n = \lambda_{i,j}^{n-1} - \Delta N A\left(\varepsilon_{i,j}^n\right)^m. \tag{13}$$

(Silling and Askari 2014) introduces two techniques – implicit strain simulation and time mapping – to speed up simulations. Both were used and are repeated here for completeness. In case of a high-cycle fatigue the bond strains from the train wheel load are below the elastic limit, so an elastic material model is used to simulate the rail. In such a case strain in a bond would change linearly between + and – loading conditions, so it is possible to simulate only the + loading condition and compute

$$s^- = Rs^+, \qquad R = \frac{P^-}{P^+}, \tag{14}$$

where R – loading ratio, P – applied load at each extreme. The cyclic strain is then given by:

$$\varepsilon = |s^+ - s^-| = |(1-R)s^+|. \tag{15}$$

Simulation time is mapped against the current cycle using a linear mapping:

$$N = \frac{t}{\tau}, \tag{16}$$

where τ is a constant. Then remaining life change in current simulation time is found through:

$$\frac{\Delta\lambda}{\Delta t} = \frac{\Delta\lambda}{\Delta N}\frac{\Delta N}{\Delta t}. \tag{17}$$

MODEL OF A RAIL

The model was discretized using meshless method introduced in (Silling and Askari

2005). Each node has a position in 3D space and describes some amount of volume around it. The edge length of a node was 0.001m and the horizon $\delta = 0.00201\text{m}$. The mesh is rather coarse and the horizon rather short, these values were selected to reduce computational expense, because here the preliminary results of a larger work are presented. In this study a model of UIC60 profile rail head was used. Due to irregular form of the rail head, nodes were not perfectly cubic; however, differences were insignificant near the middle of the rail head and increased only slightly near the gauge corners. The shape of the rail head was first created with solid hexahedral elements in finite element (FE) program Ansys, then element centroids and volumes were exported to a text file to be used as a mesh for Peridigm. Movement in vertical (y) direction was fixed for a layer of nodes with thickness δ at the bottom of the rail head, additionally damage was forbidden for nodes less than 3δ from bottom, to avoid unphysical behavior near the boundary conditions.

Since applied loads didn't cause the material to exceed its yield strength, an elastic material model was used, it's properties: density – 7850 kg/m^3, Poisson's ratio – 0.3, Young's modulus – 210 GPa. The instructions on how to obtain damage model parameter values are included in (Silling and Askari 2014), they were applied to test data presented in (Scutti et al., 1984). While the data were quite old, they were used, because all four fatigue model parameters could be estimated from just one data source, since both E-N curves and Paris law plots are presented. Fatigue damage model parameters were: A_1 – 426.00, m_1 – 2.77, A_2 – 3249.00, m_2 – 4.00. The model switched from phase I to phase II, when damage at a node reached 40%. Also, a linear time mapping was used, with τ equal to 0.001 till 21'000 cycles, 0.01 till 26'200 cycles, and 0.1 till 26670th cycle.

TRAIN WHEEL LOADING

Two different train wheel loadings were applied – vertical pressure and surface shear traction. They were obtained from (Wei et al. 2016) Fig. 5f and 6f, which show elastic pressure and elastic surface shear traction respectively. Loads were applied to a single layer of nodes at the middle of rail head's top surface, with a loading ratio $R = 0$. The wheel-rail contact area (Fig. 4f in (Wei et al. 2016)) was approximated with an ellipse whose half-axis were a=0.0066m, c = 0.006386m. The elastic pressure was approximated by an ellipsoid with half-axis a=0.0066m, c = 0.006386m, b = 1.116GPa, then the value at each node was calculated from ellipsoid formula and converted to force density. Shear traction forces change based on the location of a node in the contact area, so they were described by four tri-linear functions (Q1 to Q4). First, nodes were split into seven intervals based on their transversal location (z coordinate), second a tri-linear shear traction function was selected based on the interval, finally shear traction value was calculated and converted to force density. Table 1 shows interval limits and corresponding surface shear traction functions, Fig. 1 presents the surface shear traction functions.

RESULTS

Simulation ran for 26'670 cycles. Fig. 2 shows damage in the rail heads cross-section parallel to the longitudinal direction. First bonds break before 14'000$^{\text{th}}$ cycle, then

damage zone under applied loads expands till at 22'600th cycle node reaches 40% damage (not showed in Fig. 2.), and its neighborhood gets switched to phase II. Damage develops quite rapidly after that, leading to near complete damage (80%) at a node at cycle 26'670. Most of the broken bonds are concentrated under the maximum pressure as expected, because it creates larger bond strains. This simulation shows a very fast onset of damage that doesn't grow into longer cracks, instead damage is contained under the load area. However, it can be seen in Fig. 2 that damage extends forward under the surface forming the beginning of a squat. Longer simulations are needed to see if damage really expands in that direction. Fig. 3 shows damage in cross-section perpendicular to the longitudinal direction. The damage is nearly symmetrical at 20'000 cycles, but asymmetrical at 26'670 cycles. Most likely this is caused by the iterative solver converging to slightly different values and the mesh not being completely symmetric.

Additionally, Fig. 3 (b) shows that the top layer of nodes has broken off the following layers and penetrated them, which is an unphysical behavior. Since a large (>80%) number of bonds are broken for the top layer and loads are applied only to this layer, they no longer are distributed further down. This is the likeliest explanation for why cracks do not grow into longer squats. This problem could be remedied with finer mesh, because the same loads will be distributed over larger number of nodes, resulting in less deformation at each node and, therefore, bond. Applying loads to a thicker layer could help distribute the wheel loading in way that's closer to real life conditions. It was suggested in (Macek and Silling 2007) that loads are applied to a layer equal to the horizon. Finally, selecting longer horizon could help distribute loading to lower layers.

CONCLUSIONS

Peridynamic theory can be used to simulate rolling contact fatigue damage in a railway rail. The maximum damage will occur under the maximum pressure values as expected. The simulation showed onset of a rail squat, however simulations limitations didn't allow author's to further explore it. To remedy this boundary conditions must be applied in a way that ensures continuous load transfer to lower layers, even after surface layer sustains large damage.

REFERENCES

Baber, Forrest and Ibrahim Guven. 2017. "Solder Joint Fatigue Life Prediction Using Peridynamic Approach." *Microelectronics Reliability* 79:20–31. Retrieved (https://doi.org/10.1016/j.microrel.2017.10.004).

Bobaru, Floriin, John T. Foster, Philippe H. Geubelle, and Stewart A. Silling. 2016. *Handbook of Peridynamic Modeling*. CRC Press.

Bobaru, Florin, Youn Doh Ha, and Wenke Hu. 2012. "Damage Progression from Impact in Layered Glass Modeled with Peridynamics." *Central European Journal of Engineering* 2(4):551–61.

Bobaru, Florin and Guanfeng Zhang. 2016. "Why Do Cracks Branch? A Peridynamic Investigation of Dynamic Brittle Fracture." *International Journal of Fracture*. Retrieved (http://link.springer.com/10.1007/s10704-015-0056-8).

Colavito, Kyle. 2013. “Peridynamics for Failure and Residual Strength Prediction of Fiber-Reinforced Composites.” Retrieved (http://search.proquest.com/docview/1475241115?accountid=45156).

Gerstle, WH, N. Sau, and N. Sakhavand. 2009. “On Peridynamic Computational Simulation of Concrete Structures.” *ACI Special Publication* (February 2016). Retrieved (http://www.di.uson.mx/departamentos/dicym/images/doc/SP_265_11.pdf).

Hu, Y. L. L., N. V. V. De Carvalho, and E. Madenci. 2015. “Peridynamic Modeling of Delamination Growth in Composite Laminates.” *Composite Structures* 132:610–20. Retrieved (http://linkinghub.elsevier.com/retrieve/pii/S0263822315004626).

Hu, Y., E. Madenci, and N. Phan. 2017. “Peridynamics for Predicting Damage and Its Growth in Composites.” 1214–26.

Ishida, Makoto. 2013. “Rolling Contact Fatigue (RCF) Defects of Rails in Japanese Railways and Its Mitigation Strategies.” *Electronic Journal of Structural Engineering* 13(1):67–74.

Jung, Jeehyun and Jongwon Seok. 2016. “Fatigue Crack Growth Analysis in Layered Heterogeneous Material Systems Using Peridynamic Approach.” *Composite Structures* 152:403–7. Retrieved (http://dx.doi.org/10.1016/j.compstruct.2016.05.077).

Jung, Jeehyun and Jongwon Seok. 2017. “Mixed-Mode Fatigue Crack Growth Analysis Using Peridynamic Approach.” *International Journal of Fatigue* 103:591–603. Retrieved (http://dx.doi.org/10.1016/j.ijfatigue.2017.06.008).

Kaewunruen, S., ‘Identification and prioritization of rail squat defects in the field using rail magnetisation technology’, Proceedings of SPIE - The International Society for Optical Engineering 9437, 94371H (2015). doi: 10.1117/12.2083851

Kaewunruen, S., ‘Discussion of “Field Test Performance of Noncontact Ultrasonic Rail Inspection System” by Stefano Mariani, Thompson Nguyen, Xuan Zhu, and Francesco Lanza di Scalea’, Journal of Transportation Engineering, Part A: Systems 144 (4), 07018001 (2018). doi: 10.1061/JTEPBS.0000134

Kaewunruen, S., Ishida, M.: Field monitoring of rail squats using 3D ultrasonic mapping technique. J. Can. Inst. Non-destr. Eval. (invited), 35(6), 5–11 (2014).

Kaewunruen S. and Ishida M. ‘Rail squats: understand its causes, severity, and non-destructive evaluation techniques,’ Proceedings of the 20th National Convention on Civil Engineering, Pattaya, Thailand, 8-10 July, (2015). (Best Paper Award in Infrastructure Engineering), [URL https://works.bepress.com/sakdirat_kaewunruen/56/]

Kaewunruen, S., Ishida, M.: In Situ Monitoring of Rail Squats in Three Dimensions Using Ultrasonic Technique. Experimental Techniques. 40(4): 1179-1185 (2016).

Kaewunruen, S., Ishida, M., Marich, S., “Dynamic wheel-rail interaction over rail squat defects,” Acoustics Australia, 43(1): 97-107, (2015). doi: 10.1007/s40857-014-0001-4

Kaewunruen, S. and A. M. Remennikov. 2010. “Dynamic Properties of Railway Track and Its Components: Recent Findings and Future Research Direction.” *Insight - Non-Destructive Testing and Condition Monitoring* 52(1):20–22. Retrieved (http://www.ingentaconnect.com/content/bindt/insight/2010/00000052/00000001/art00006).

Kaewunruen, Sakdirat and Alex M. Remennikov. 2009. “Progressive Failure of Prestressed Concrete Sleepers under Multiple High-Intensity Impact Loads.” *Engineering Structures* 31(10):2460–73. Retrieved (http://dx.doi.org/10.1016/j.engstruct.2009.06.002).

Kaewunruen, S., Remennikov, A.M.: Current state of practice in railway track vibration isolation: an Australian overview, Australian Journal of Civil Engineering 14(1), pp. 63-71 (2016).

Kilic, B., A. Agwai, and E. Madenci. 2009. “Peridynamic Theory for Progressive Damage Prediction in Center-Cracked Composite Laminates.” *Composite Structures* 90(2):141–51. Retrieved (http://dx.doi.org/10.1016/j.compstruct.2009.02.015).

Lihlewood, David, Michael Parks, John Mitchell, and Stewart Silling. 2013. “The Peridigm Framework for Peridynamic Simulations.” (July).

Macek, Richard W. and Stewart A. Silling. 2007. “Peridynamics via Finite Element Analysis.” *Finite Elements in Analysis and Design* 43(15):1169–78.

Madenci, Erdogan and Erkan Oterkus. 2014. *Peridynamic Theory and Its Applications*. New York, NY: Springer New York. Retrieved (http://link.springer.com/book/10.1007/978-1-4614-8465-3).

De Meo, D., C. Diyaroglu, N. Zhu, E. Oterkus, and M. Amir Siddiq. 2016. “Modelling of Stress-Corrosion Cracking by Using Peridynamics.” *International Journal of Hydrogen Energy* 41(15):6593–6609. Retrieved (http://dx.doi.org/10.1016/j.ijhydene.2016.02.154).

Oterkus, Erkan, Ibrahim Guven, and Erdogan Madenci. 2010. “Fatigue Failure Model with Peridynamic Theory.” in *2010 12th IEEE Intersociety Conference on Thermal and Thermomechanical Phenomena in Electronic Systems, ITherm 2010*.

Parks, Michael L., David J. Littlewood, John a Mitchell, and Stewart a Silling. 2012. *Peridigm Users ’ Guide*.

Perré, Patrick, Giana Almeida, Mehdi Ayouz, and Xavier Frank. 2015. “New Modelling Approaches to Predict Wood Properties from Its Cellular Structure: Image-Based Representation and Meshless Methods.” *Annals of Forest Science*. Retrieved (http://link.springer.com/10.1007/s13595-015-0519-0).

Remennikov, Alex M. and Sakdirat Kaewunruen. 2008. “A Review of Loading Conditions for Railway Track Structures Due to Train and Track Vertical Interaction.” *Structural Control and Health Monitoring* 15(2):207–34. Retrieved (10.1002/stc.227%0A).

Scutti, J. J., R. M. Pelloux, and R. Fuquen-Moleno. 1984. “FATIGUE BEHAVIOR OF A RAIL STEEL.” *Fatigue & Fracture of Engineering Materials and Structures* 7(2):121–35. Retrieved (http://doi.wiley.com/10.1111/j.1460-2695.1984.tb00410.x).

Shen, Feng, Qing Zhang, and Dan Huang. 2013. “Damage and Failure Process of Concrete Structure under Uniaxial Compression Based on Peridynamics Modeling.” 2013.

Silling, S. A. 2000. “Reformulation of Elasticity Theory for Discontinuities and Long-Range Forces.” *Journal of the Mechanics and Physics of Solids* 48(1):175–209.

Silling, S. A. and E. Askari. 2005. “A Meshfree Method Based on the Peridynamic

Model of Solid Mechanics." *Computers and Structures* 83(17–18):1526–35.
Silling, S. A., M. Epton, O. Weckner, J. Xu, and E. Askari. 2007. "Peridynamic States and Constitutive Modeling." *Journal of Elasticity* 88(2):151–84.
Silling, S. A. and R. B. Lehoucq. 2010. "Peridynamic Theory of Solid Mechanics. Advances in Applied Mechanics." *Advances in Applied Mechanics* 44:73–168.
Silling, Stewart and Abe Askari. 2014. *Peridynamic Model for Fatigue Cracks SANDIA REPORT SAND2014-18590*. Albuquerque. Retrieved (http://docs.lib.purdue.edu/ses2014/mss/cfm/22/).
Wei, Zilong, Zili Li, Zhiwei Qian, Rong Chen, and Rolf Dollevoet. 2016. "3D FE Modelling and Validation of Frictional Contact with Partial Slip in Compression–shift–rolling Evolution." *International Journal of Rail Transportation* 4(1):20–36. Retrieved (http://dx.doi.org/10.1080/23248378.2015.1094753).
Yaghoobi, Amin and Mi G. Chorzepa. 2015. "Meshless Modeling Framework for Fiber Reinforced Concrete Structures." *Computers & Structures* 161:43–54. Retrieved (http://www.sciencedirect.com/science/article/pii/S0045794915002485).
Zhang, Guanfeng, Quang Le, Adrian Loghin, Arun Subramaniyan, and Florin Bobaru. 2016. "Validation of a Peridynamic Model for Fatigue Cracking." *Engineering Fracture Mechanics* 162:76–94. Retrieved (http://dx.doi.org/10.1016/j.engfracmech.2016.05.008).

TABLES

Table 1. Interval limits in transverse direction and their tri-linear surface shear traction functions.

Interval	Interval start transversal coordinate, m	Interval end transversal coordinate, m	Tri-linear Surface Shear Traction Function
1	-0.006386	-0.005	Q4
2	-0.005	-0.003	Q3
3	-0.003	-0.001	Q2
4	-0.001	0.001	Q1
5	0.001	0.003	Q2
6	0.003	0.005	Q3
7	0.005	0.006386	Q4

FIGURES

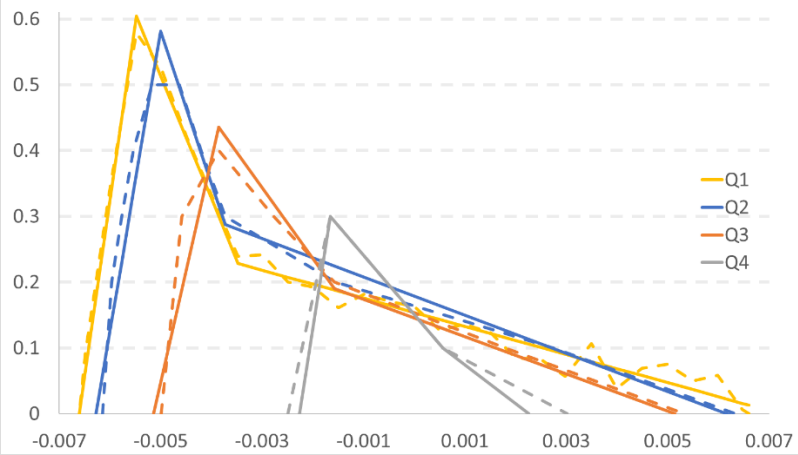

FIG. 1. Surface shear traction (GPa) vs the x coordinate of a node (m). Dashed lines show data from (Wei et al. 2016) **and solid lines show the fitted tri-linear functions (Q1 to Q4).**

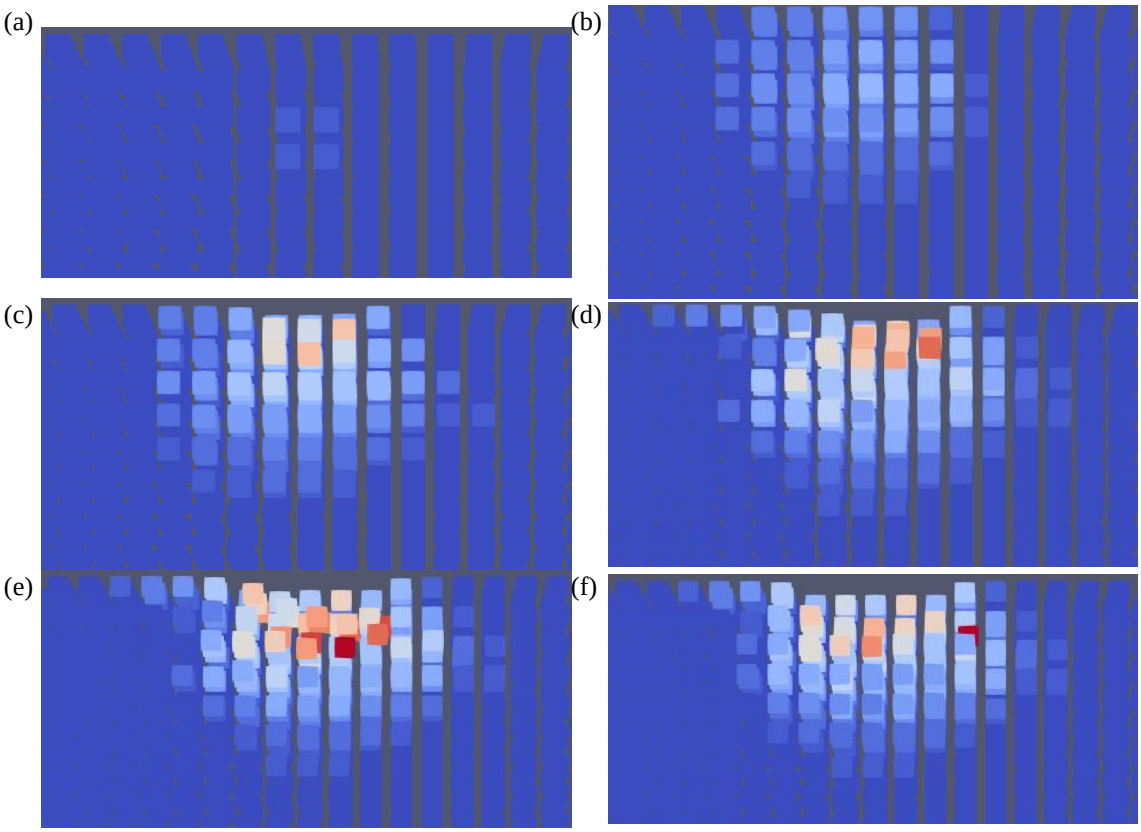

FIG. 2. Cross-section (plane parallel to the longitudinal direction) at the middle

of the rail head showing damage from rolling contact fatigue at (a) - 14’000 cycles, (b) – 21’000, (c) – 25’000, (d) – 26’200, (e) – 26’580, (f) – 26’670. Rolling direction is to the right and only damaged zone is shown. Blue color – less damage, red – more damage.

(a) (b)

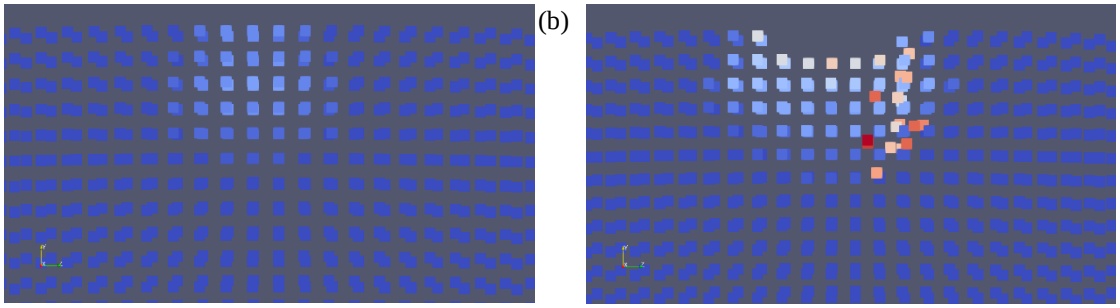

FIG. 3. Cross-section (plane normal to longitudinal direction) at the middle of rail head (center of the applied load) showing damage from rolling contact fatigue at (a) - 20’000 cycles, (b) – 26’670. Color scheme indicates damage at a node with blue – less damage, red – more damage.